AIAA 2009-3570

39th AIAA Fluid Dynamics Conference
22 - 25 Jun 2009, Grand Hyatt Hotel, San Antonio, Texas

Richtmyer-Meshkov instability in reactive mixtures

M. Ungarala * Luca Massa†

This paper analyzes the effect of reactivity on the Richtmyer-Meshkov instability with particular emphasis on the velocity and wave number scaling and on the effect of free detonation instability modes on the interface corrugation rate. The analysis is performed by solving numerically for the first order perturbation generated by the shock-induced acceleration of an initially corrugated interface. The results show a profound effect of the reactivity on both the short time growth rate and the long time linear regime.

I. Introduction

This paper analyzes the role of mixture reactivity on the dynamics of the Richtmyer-Meshkov instability (RMI) (see Richtmyer[1] for a more detailed description on the non-reactive problem). The phenomenon is of physical importance in the context of detonation initiation and baroclinic mixing. Previous attempts to model the RMI in reactive fluids lack a thorough examination of the mixture thermo-chemical properties on the surface deformation rate, of the induction-disturbance scaling, and of the interaction between the detonation global instability and the interface convective instability.

A peculiar difference between reactive and nonreactive problems is the wave number scaling. Khoklov, *et al.*[2,3] analyzed the RMI resulting from flame shock interaction. They note the absence of fine scales interface disturbances in burning computations, and conjecture that the flame consumes the small scales. The Richtmyer shock problem has no geometrical length scale, so that, in the non-reactive case, the normalized growth rate of an interface disturbance scales linearly with the disturbance wave number. The premixed combustion problem that supports detonation initiation has, in its most simple form, the induction length as associated scale. The relationship between induction and disturbance wave number introduces a scaling parameter, Massa and Lu.[4]

It is widely acknowledged that non-reacting shocks are stable to linear perturbations, while detonations are unstable for realistic values of the heat release. In the non-reactive Richtmyer-Meshkov problem, the interface deforms with a linear rate, while the shocks relax toward the unperturbed state with an exponential decay. In the reactive case, for a time-unstable detonation, the resonant interaction between surface deformation and detonation instability may support super-linear growth rates of interface disturbances.

Instability patterns associated with the RMI play a fundamental role in the mixing rate through the strain driven gradient steepening at the interfaces. The contribution of the initial patterns to the instantaneous mixing rate was measured to be up to 80% of the peak mixing rate, in non-reactive measurements Tomkins, *et al.*[5] On the other hand, for reactive mixtures, we expect the scaling effect to alter shock induced mixing, and favor the process at selected wave numbers.

In this paper we present a linear stability analysis of the RMI supporting detonation initiation. This analysis focuses on scaling of the interface growth rate with the perturbation wave number under combustion conditions, and on the coupling between detonation front and interface instabilities. This draft documents the method, numerical convergence of the solution, and preliminary results obtained assuming infinitely fast kinetics.

*Graduate Student, Mechanical and Aerospace Engineering, University of Texas at Arlington
†Assist. Prof., 500 W. First St., WH 214, Arlington, TX, 76019. email: massa@uta.edu. phone: 817-272-0125.

II. The problem

The objective of this section is to identify the dynamics of a perturbation of a planar interface between two fluids of different density when subject to instantaneous shock acceleration. We shall do so by assuming that the perturbation is much smaller than the base flow, and thus by linearizing the dynamic equations. The focus of the research is on the effect of the reactivity of the mixture on perturbation growth.

Consider a planar shock incident on a interface that separates two immiscible fluids of different density Fig. 1(a). The two dimensional plane has Cartesian coordinates x and y, to which correspond unitary vectors $\vec{i}$ and $\vec{j}$. At time $t = t_0$ the shock hits the interface and a reflected and a transmitted corrugated shocks depart from the point of impact Fig. 1(b). There are three interfaces in the system, the reflected shock labeled as (r), the transmitted shock labeled as (t), and the contact interface labeled as (I). The interfaces move with time/space dependent velocities, $W_r(t, y)$, $W_t(t, y)$ and $W_I(t, y)$ with directions indicated in Fig. 1(b). The reflected-transmitted shock system divides the space in 4 regions labeled in Fig. 1(b) as region(0) to the left of the transmitted shock, region(1), region(2) and region(3) to the right of the reflected shock. Only one of the two fluids, that in region(1), is assumed to be reactive; this configuration models a detonation initiation by shock impingement.

We seek to evaluate the time dependent solution to the problem, *i.e.*, the pressure p, velocity vector $\vec{u} \equiv u\vec{i} + v\vec{j}$, the density ρ, and reaction progress variable λ. In a vector form we write the solution vector as

$$P(x, y, t) = [p, u, v, \rho, \lambda]^T. \tag{1}$$

The solution vector is expanded in the sum of a base solution (zeroth order solution) and a perturbation (first order solution):

$$P(x, y, t) = P^0(x, y, t) + P^1(x, y, t). \tag{2}$$

Note that if there were no combustion, the zeroth order would not be a function of the spatial coordinates or the time.

III. Governing Equations

The governing equations are the Euler equations for a reactive flow. The four regions of the space are connected using the Rankine-Hugoniot conditions at the 3 interfaces. We shall also consider the incident shock, labeled as (inc), when solving for the flow. The Rankine-Hugoniot equations are written in terms of local conditions at the interface. First, for each point (P) on the interface we define a local reference system (t,n) moving at the interface speed and aligned with it, as shown in Fig. 2. The normal and tangential components of the velocity vector with respect to the local coordinate system (t,n) are:

$$u_n = (u - W)\cos\theta + v\sin\theta, \tag{3a}$$

$$u_t = -u\sin\theta + v\cos\theta. \tag{3b}$$

Next, for each interface we define a jump operator $[\cdot]$ that yields the difference between the quantity at the right of the interface (R) minus the quantities at the left of it (L). Additionally, we introduce the assumption of thermally and calorically perfect gases with isentropic index γ, and introduce the total enthalpy

$$H = \frac{\gamma}{\gamma - 1}\frac{p}{\rho} - Q\lambda + \frac{1}{2}\left(u_n^2 + u_t^2\right).$$

The Rankine-Hugoniot relations are written as:

$$[\rho u_n] = 0 \tag{4a}$$

$$\left[p + \rho u_n^2\right] = 0 \tag{4b}$$

$$[u_t] = 0 \tag{4c}$$

$$[H] = 0 \tag{4d}$$

$$[\lambda] = 0. \tag{4e}$$

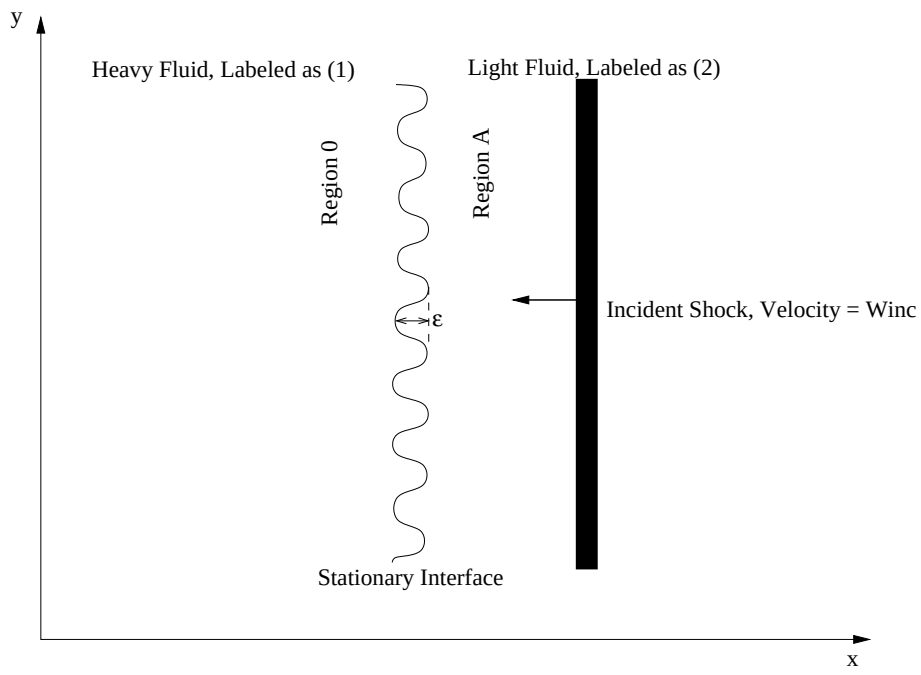

(a) Incident Shock.

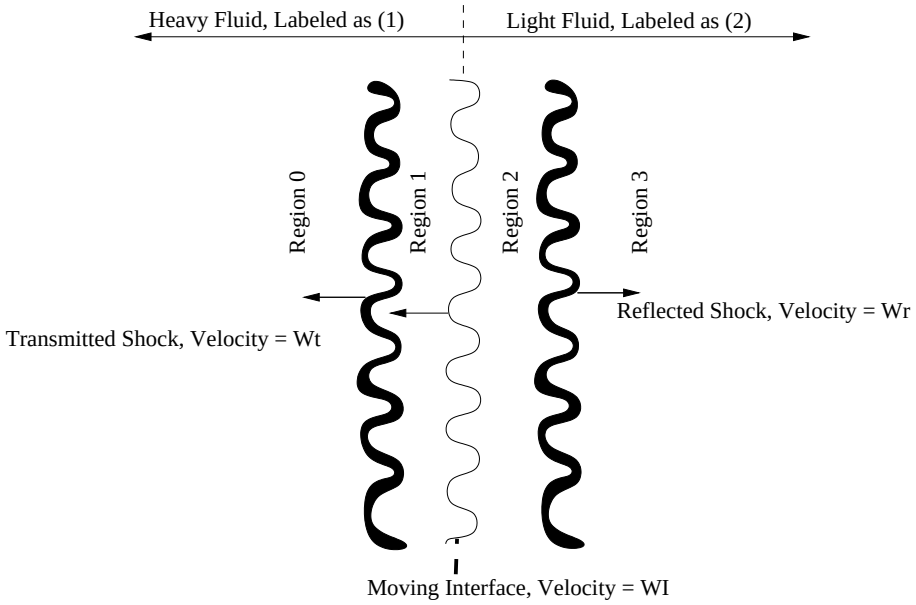

(b) Shock system after reflection.

Figure 1. Reflected and transmitted shocks.

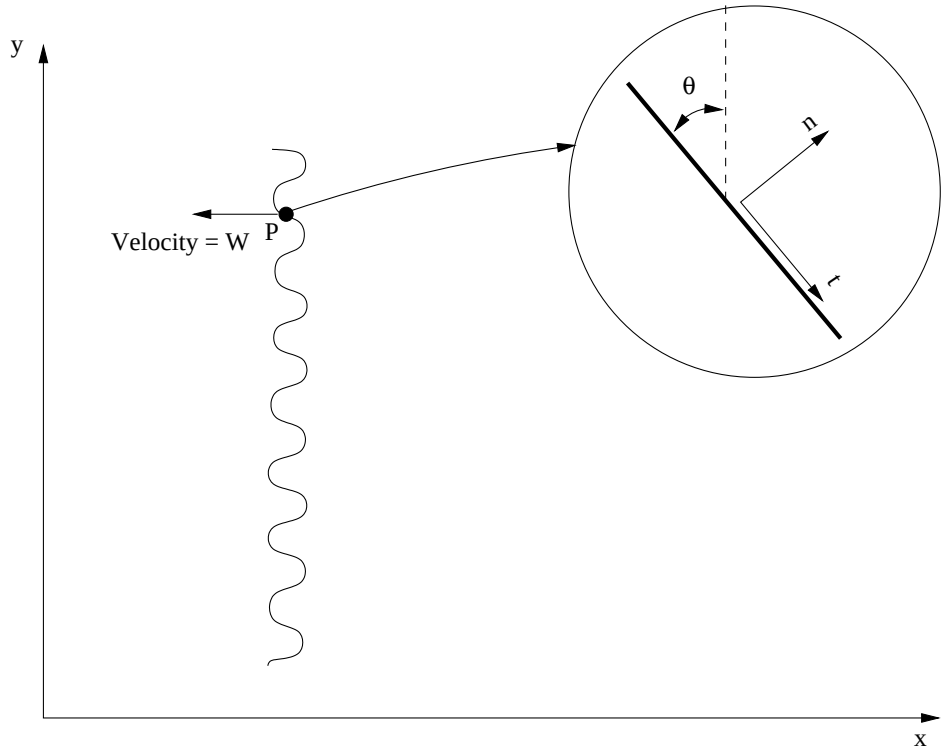

Figure 2. Local conditions at any interface (shocks, or contact discontinuity.

IV. Zeroth order boundary conditions

At the zeroth order the surface corrugation is zero, and thus $\theta = 0$. Equations (4c) and (4e) are therefore decoupled from the rest of equation (4), and imply that the tangential velocity and the species mass fractions are identical on both sides of the interface (hence the value of the progress variable is set to zero on both sides). The remaining three equations can be solved for the interface velocity W, the density ρ and the fluid velocity u on one side of the interface once the same conditions on the other side plus the pressure on both sides are given. It is customary to solve the equations for the density ratio $\mathscr{X}_\rho \equiv \frac{\rho_L}{\rho_R}$ in terms of the (assigned) pressure ratio $\mathscr{X}_p \equiv \frac{p_L}{p_R}$. To do so, we shall introduce a utility variable, $g = \frac{\gamma+1}{\gamma-1}$. For the sake of example, we assume that we want to find the solution on the left side (L) in terms of that on the right side (R) and $\mathscr{X}_p$; the opposite case is easily determined. We find:

$$\mathscr{X}_\rho = \frac{1 + g\mathscr{X}_p}{g + \mathscr{X}_p}, \tag{5a}$$

$$u_{nL} = \pm\sqrt{\frac{p_R}{\rho_R}}\sqrt{\frac{\mathscr{X}_p - 1}{\mathscr{X}_\rho\left(\mathscr{X}_\rho - 1\right)}}, \tag{5b}$$

$$u_{nR} = \mathscr{X}_\rho u_{nL}. \tag{5c}$$

In order to find the velocity in the original coordinate system (x,y)[a], we eliminate the shock velocity by writing

$$u_{nR} = u_R - W \text{ and } u_{nL} = u_L - W \implies u_L = u_R + u_{nL} - u_{nR}.$$

[a]Remember we are solving for the left side given the right side.

Therefore, the final equation is

$$u_L = u_R \pm \sqrt{\frac{p_R}{\rho_R}}\,(\mathscr{X}_p - 1)\sqrt{\frac{g-1}{1+g\mathscr{X}_p}}. \tag{6}$$

Both solutions (+) and (-) are mathematically possible. Physically the sign is determined by looking at the direction toward which the shock propagates.

The Rankine-Hugoniot equations are valid also at the contact interface (I). The solution method is slightly different, because the essence of a contact discontinuity is that the velocity on either side of the interface is equal to the velocity of the interface, *i.e.*, there is no fluid crossing the interface:

$$u_L = u_R = W \implies u_{nL} = u_{nR} = 0. \tag{7}$$

Therefore, only equation (4b) of equation (4) is meaningful, and yields

$$p_L = p_R, \tag{8}$$

equation (8) plus the two equations $u_L = W$ and $u_R = W$ are the only equations we shall write for the interface. Notice that we have

$$\rho_L \neq \rho_R \; v_L \neq v_R \text{ and } \lambda_L \neq \lambda_R.$$

Therefore, for a contact discontinuity, we cannot obtain the solution on one side given that on the other side and the pressure ratio.

V. Euler Equations

The reactive Euler equations control the time evolution of the solution in regions (1) and (2), *c.f.*, Fig. 1(b). We start with the conservative variable formulation,

$$\frac{\partial \mathscr{Q}}{\partial t} + \frac{\partial F}{\partial x} + \frac{\partial G}{\partial y} + R_1 = 0, \tag{9}$$

where,

$$\mathscr{Q} = \begin{bmatrix} \rho \\ \rho u \\ \rho v \\ \rho\left[\frac{1}{\gamma-1}\frac{p}{\rho} - Q\lambda + \frac{1}{2}\left(u^2+v^2\right)\right] \\ \rho\lambda \end{bmatrix},\; F = \begin{bmatrix} \rho u \\ p+\rho u^2 \\ \rho uv \\ \rho uH \\ \rho u\lambda \end{bmatrix},\; G = \begin{bmatrix} \rho v \\ \rho uv \\ p+\rho v^2 \\ \rho vH \\ \rho v\lambda \end{bmatrix} \text{ and } R_1 = \begin{bmatrix} 0 \\ 0 \\ 0 \\ 0 \\ -\rho\dot{\omega} \end{bmatrix}, \tag{10}$$

and $\dot{\omega} \equiv (1-\lambda)\,A_\omega \exp -E_\omega \rho/p$ is the rate of destruction of mass of reactant per unit mass of mixture. It is useful to transform the Euler equations in primitive variables, P *c.f.*, equation (1). To do so we evaluate a set of Jacobian matrices, $Q_P \equiv \frac{\partial \mathscr{Q}}{\partial P}$, $A_1 \equiv \frac{\partial F}{\partial P}$ and $B_1 \equiv \frac{\partial G}{\partial P}$, write the Euler equations as

$$\frac{\partial P}{\partial t} + Q_P^{-1}A_1\frac{\partial P}{\partial x} + Q_P^{-1}B_1\frac{\partial P}{\partial y} + Q_P^{-1}R_1 = 0, \tag{11}$$

denote

$$A \equiv Q_P^{-1}A_1,\; B \equiv Q_P^{-1}B_1 \text{ and } R \equiv Q_P^{-1}R_1,$$

and finally write

$$\frac{\partial P}{\partial t} + A\frac{\partial P}{\partial x} + B\frac{\partial P}{\partial y} + R = 0, \tag{12}$$

where the matrices are given by,

$$A \equiv \begin{pmatrix} u & \gamma p & 0 & 0 & 0 \\ \frac{1}{\rho} & u & 0 & 0 & 0 \\ 0 & 0 & u & 0 & 0 \\ 0 & \rho & 0 & u & 0 \\ 0 & 0 & 0 & 0 & u \end{pmatrix}; B \equiv \begin{pmatrix} v & 0 & \gamma p & 0 & 0 \\ 0 & v & 0 & 0 & 0 \\ \frac{1}{\rho} & 0 & v & 0 & 0 \\ 0 & 0 & \rho & v & 0 \\ 0 & 0 & 0 & 0 & v \end{pmatrix} R \equiv \begin{pmatrix} -(\gamma-1)Q\rho\dot{\omega} \\ 0 \\ 0 \\ -\dot{\omega} \end{pmatrix}. \tag{13}$$

V.A. Coordinate transformation

A coordinate transformation is necessary to map the time dependent solution domain in a stationary one. We concentrate on regions (1) and (2). We transform the domain between the two moving shocks into a stationary domain between two flat shocks. The mapping is illustrated in Fig. 3. Consider a region, either (1)

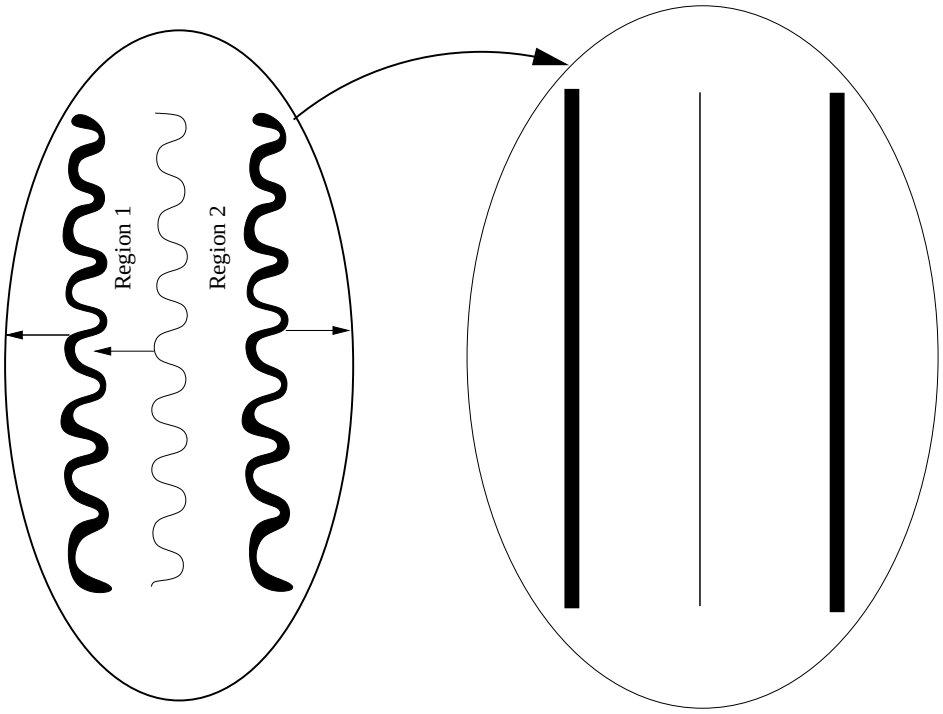

Figure 3. Schematic of the mapping.

or (2), and assume that the coordinate of the two interfaces that delimit it are given as $x_1(y,t)$ and $x_2(y,t)$ for the left and right interfaces, respectively. We define a new coordinate system (τ, ξ and η) related to (t, x and y) by

$$x = x_1 + \frac{x_2 - x_1}{2}(\xi + 1), \quad \xi \in [-1, 1], \tag{14a}$$

$$y = \eta, \quad \eta \in [-\infty, \infty], \tag{14b}$$

$$t = \tau, \quad \tau \in [0, \infty]. \tag{14c}$$

For the sake of a short hand notation, we define three auxiliary variables,

$$\beta_1 = -\frac{\xi - 1}{2}, \ \beta_2 = 1 - \beta_1 \text{ and } \delta = \sum_{j=1}^{2} \frac{d\beta_j}{d\xi} x_j. \tag{15}$$

As customary in coordinate transformations, the next step is to determine derivatives with respect to ($t,\ x$ and y) in terms of derivatives with respect to ($\tau,\ \xi$ and η). For any variable $\psi\,(t,\ x,\ y)$, we find

$$\frac{\partial \psi}{\partial x} = \frac{\partial \psi}{\partial \xi}/\delta \tag{16a}$$

$$\frac{\partial \psi}{\partial t} = \frac{\partial \psi}{\partial \tau} - \left(\sum_{j=1}^{2} \beta_j \frac{\partial x_j}{\partial t}\right) \frac{\partial \psi}{\partial \xi}/\delta \tag{16b}$$

$$\frac{\partial \psi}{\partial y} = \frac{\partial \psi}{\partial \eta} - \left(\sum_{j=1}^{2} \beta_j \frac{\partial x_j}{\partial y}\right) \frac{\partial \psi}{\partial \xi}/\delta. \tag{16c}$$

V.B. Linearized equations

Substitution of the mapping relations, equation (16), into the Euler equation, equation (12), yields a set of non-linear equations. Using equation equation (2) for the primitive variables, and collecting term of equal perturbation order yields two linear equations, one for the zeroth order, P^0, and one for the first order perturbation, P^1. In the non-reactive case, the zeroth order equation reduces to $P^0 = \text{const}$ over both regions (1) and (2). In the reactive case, the equation is non-linear and given by

$$\frac{\partial P^0}{\partial \tau} + \left(\frac{A^0}{\delta^0} - \sum_{j=1}^{2} \frac{\beta_j}{\delta^0} W_j^0 \mathrm{I}\right) \frac{\partial P^0}{\partial \xi} + R\left(P^0\right) = 0. \tag{17}$$

Before discussing the first order equation, we adopt a nomenclature similar to Richtmyer's[1] equations 6-8, and set,

$$x_j = W_j^0 t + a_j(t, y). \tag{18}$$

The time derivatives of the corrugation terms with respect to the time $\dot{a}_j$ will be identified as deformation rates, *i.e.*, $\dot{a}_I$ is the interface deformation rate. Thus, we obtain the following expansions,

$$\delta^0 = \left(\sum_{j=1}^{2} \frac{d\beta_j}{d\xi} W_j^0\right) t, \qquad \delta^1 = \sum_{j=1}^{2} \frac{d\beta_j}{d\xi} a_j(t, y). \tag{19}$$

In the linearized analysis we assume (for both reactive and non-reactive fluids) the $y \equiv \eta$ direction to be homogeneous, thus the zeroth order solution does not depend on η. Derivatives of the first order perturbation with respect to η are determined by multiplying the value of the function by the term ik, where i is the imaginary unit and k is the wave number of the perturbation, *i.e.*,

$$\frac{\partial \psi}{\partial \eta} = ik\psi.$$

The first order perturbation equation becomes after some manipulation,

$$\begin{aligned} \frac{\partial P^1}{\partial \tau} + \frac{\delta^1}{\delta^0}\left(\frac{\partial P^0}{\partial \tau} + R\left(P^0\right)\right) - \left(\sum_{j=1}^{2} \frac{\beta_j}{\delta^0} \dot{a}_j\right) \frac{\partial P^0}{\partial \xi} - ik\left(\sum_{j=1}^{2} \frac{\beta_j}{\delta^0} a_j\right) B^0 \frac{\partial P^0}{\partial \xi} \\ + \left(\frac{A^0}{\delta^0} - \sum_{j=1}^{2} \frac{\beta_j}{\delta^0} W_j^0 \mathrm{I}\right) \frac{\partial P^1}{\partial \xi} + ikB^0 P^1 + \frac{\partial R}{\partial P} P^1 + \frac{A^1 \frac{\partial P^0}{\partial \xi}}{\delta^0} = 0, \end{aligned} \tag{20}$$

where I is the identity matrix.

V.C. Initial Conditions

The initial conditions are given at $t = 0$, $\delta^0 = 0$. The zeroth order solution is taken piecewise constant in regions (1) and (2). The shock and contact discontinuity jump conditions yield the values for the flow variables. The time derivatives at the initial time is evaluated by taking the limit for $t \to 0^+$ of equation (17). By using the l'Hôpital's rule the initial derivative $\dot{P}$ is found by solving

$$\frac{\partial \dot{P}}{\partial \tau} + \frac{A^0 - \sum_{j=1}^{2} \beta_j W_j^{0\mathrm{I}}}{\left(\sum_{j=1}^{2} \frac{d\beta_j}{d\xi} W_j^0\right)} \frac{\partial \dot{P}}{\partial \xi} + R\left(P^0\right) = 0. \tag{21}$$

where P^0, W^0 and A^0 are evaluated at the initial time. Equation (21) together with boundary conditions on $\dot{P}$ resulting from differentiating the shock jump conditions, are solved using the same discretization as for the time dependent problem. Note:

$$\frac{\partial P^0}{\partial x} = \lim_{t \to 0^+} \frac{\partial P^0}{\partial \xi} / \delta^0 \neq 0$$

leads to $\lim_{t\to 0^+} \frac{\partial \dot{P}}{\partial \xi} \neq 0$, as a consequence of the boundary conditions, which implies that

$$\lim_{t \to 0^+} \left(\frac{\partial P^0}{\partial \tau} + R\left(P^0\right) \right) \neq 0. \tag{22}$$

The initial values of the interface perturbations, $a_j,\ j = 1 \ldots, 3$, are determined by the initial instantaneous acceleration imparted by the shock to the interfaces. These perturbations are normalized by the value at the the contact discontinuity, $j = 2$, therefore,

$$a_j = \frac{1 - W_j / W_{inc}}{1 - W_2 / W_{inc}}. \tag{23}$$

The initial conditions in equation (23) are not different from those reported by Richtmyer.[1] The conclusion that the initial compression of the interface is not affected by the reactivity is rooted in the fact that the initial perturbation is assumed much smaller than any characteristic reaction length, say the half reaction distance. The non-reactive RMI analysis is valid for $\epsilon k \ll 1$, where k is the interface disturbance wave number. The present analysis requires also $Da \epsilon k \ll 1$.

The remaining conditions for the first order perturbation are determined by taking the limit of equation equation (20) for $t \to 0^+$, which corresponds with sending $\delta_0 \to 0$. The limit together with the boundary conditions yield a set of ordinary differential equations in ξ, which are solved using the same discretization as for the time dependent problem. Note that the previous result in equation (22) leads to $\lim_{t\to 0^+} \frac{\partial P^1}{\partial \xi} \neq 0$, and a non-zero initial perturbation. Physically the non-zero initial perturbation is explained by considering the passage of the incident shock through the initial perturbation. Fluid particles with different y intersect the interface at different times, leading to equation (23). When $\lim_{t\to 0^+} \frac{\partial P^0}{\partial \xi} / \delta^0 \neq 0$, *i.e.*, for reactive conditions, this yields an initial perturbation with constant but non-zero first derivative. Shock induced acceleration deposit an initial vorticity that is dependent on the spatial derivative of the post-shock field, and thus on the Damkhöler number. As a consequence, the initial surface deformation rates

$$\lim_{t \to 0^+} \dot{a}_j \neq 0,\ j = 1, \ldots, 3.$$

For the non-reactive case, only v^1 is non-zero at $t = 0$. In the reactive counterpart $\frac{\partial v^0}{\partial x} = 0$, so the initial distribution of v^1 is identical to the non-reactive analog.

The time derivative of the perturbation at $t = 0$ is found by applying the l'Hôpital's rule to the limit of equation (20) for $t \to 0^+$. The resulting ordinary differential equation is similar in structure to equation (21), and requires boundary conditions for the time derivative of the first order perturbation, which are obtained by time differentiating the perturbation of the shock jump conditions.

V.D. Scales and parameters

The pressure, density and temperature scales are the corresponding variables in region(0) of Fig. 1(b). The velocity scale is the square root of the ratio between reference pressure and density. The length scale is the inverse of the wave number k of the transversal (to the shock) disturbance. The time scale is the residence time based on the reference velocity and length.

The transition of a shock from a non-reactive to a reactive mixture will be considered in this research. The reactive mixture is in region(1) while the non-reactive gas is in region(2) of Fig. 1(b). The solution to the non-dimensional problem depends on a number of non-dimensional parameters calculated under the assumption of a steady detonation in region(1). The first four are the non-dimensional activation energy E, heat release Q, isentropic index, *gamma*, and overdrive f, defined as in Erpenbeck.[6] The isentropic index is kept constant and equal to 1.2 in all results presented in the present paper. The fifth is the Damkhöler number. Note that if reaction half distance were selected as length scale, this last parameter would be replaced by the product of perturbation wave number k and reaction half distance, $L_{1/2}$. The choice of the wave number as length parameter is due to the fact that the Richtmyer instability is dominant over the detonation intrinsic instability, and the transversal wave length is the only scale of the non-reactive problem. The sixth parameter is the initial density ratio taken across the stationary interface,Fig. 1(a), between region(A) and region(0). This parameter is labeled R^*.

The six non-dimensional parameters lead to the determination of all other non-dimensional variables that describe the system. An important variable is the Mach number of the incident wave depicted in Fig. 1(a), M_{inc}. A lower bound for this value can be determined by taking $f = 1$, $R^* \Rightarrow 0$ and varying the heat release. Such solution is plotted together with the value corresponding to $R^* = 1/2$ in Fig. 4. The plot demonstrates the large incident Mach numbers necessary to obtain a steady detonation structure in region (2).

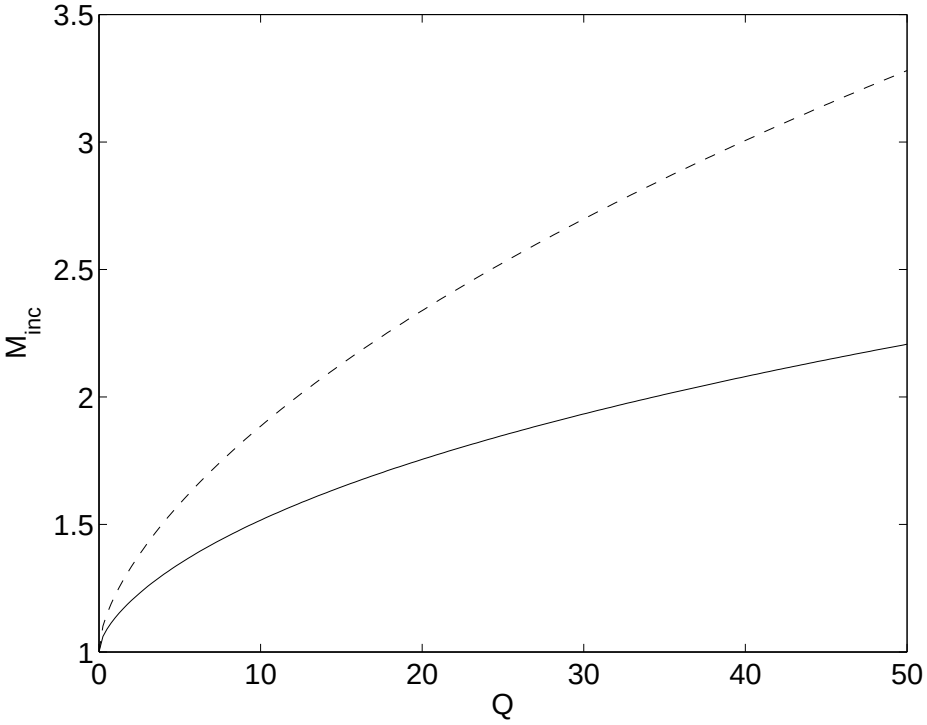

Figure 4. Incident Mach number versus heat release parameter for two density ratios: $R^* \Rightarrow 0$ solid line, and $R^* = 1/2$ dashed line.

The parameters will be varied to study their effect on the instability. The value of the overdrive will be kept constant and equal to 1.2. The value of the heat release and the activation energy will be changed at the same rate to simulate the effect of changing the unreacted stream temperature. Physical variations

of region(0) temperature correspond to either pre-heating of the mixture or the passage of multiple shocks across the interface. Therefore, we set, for simplicity, $E = Q$. A characteristic value of $E = Q$ is the threshold for longitudinal instability. This value is significant to this study because below this threshold the long-time base flow solution will approach a traveling wave in region(0), while above this value a pulsating solution is obtained. The threshold point for $\gamma = f = 1.2$ is equal to 18.39 and the growth rate is shown in Fig. 5. Note that in Fig. 5 the absence of a transversal perturbation requires that the half reaction distance is used as length scale.

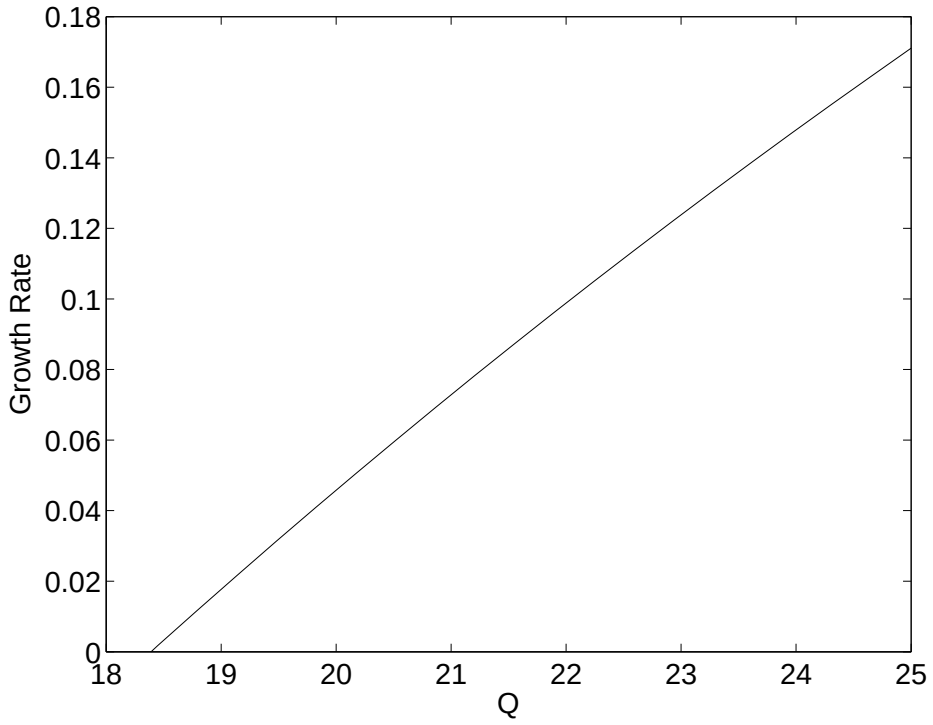

Figure 5. Growth rate of longitudinal perturbations. The positive growth rate indicates unstable waves.

As previously mentioned, the Damkhöler number represents a relationship between reaction and perturbation lengths. In this research the mixture properties have been kept constant while the temperature in region(0) and the perturbation wave number are varied. The temperature is assigned by means of the ratio $\phi_T \equiv E/25$, which means that $E_{ref} = 25$ is used as reference (*i.e.*, nominal) non-dimensional activation energy, and obviously $Q_{ref} = E_{ref}$. The perturbation wave number is given by the product $\phi_K \equiv kL_{1/2,\phi_T=1}$, which implies that the inverse of the half reaction length at $E = 25$ is used as reference wave number. The Damkhöler number is then defined as

$$Da = \frac{\int_0^{1/2} \frac{u \exp\left(-\frac{\rho E_{ref}}{p}\right)}{1-\lambda} \, \mathrm{d}\lambda}{\sqrt{\phi_T}\phi_K}, \tag{24}$$

where u, p and ρ are the customary functions of λ, Q_{ref} and f:

$$M_0 = \sqrt{\frac{f\left(\gamma^2 Q_{ref} + \sqrt{\left(\gamma^2-1\right)Q_{ref}\left(\left(\gamma^2-1\right)Q_{ref}+2\gamma\right)} + \gamma - Q_{ref}\right)}{\gamma}} \tag{25a}$$

$$p = \frac{\sqrt{\gamma\left(\gamma\left(M_0^2-1\right)^2 - 2\left(\gamma^2-1\right)\lambda M_0^2 Q_{ref}\right)} + \gamma M_0^2 + 1}{\gamma+1} \tag{25b}$$

$$u = \frac{\gamma M_0^2 - p + 1}{\sqrt{\gamma} M_0} \tag{25c}$$

$$\rho = \frac{\sqrt{\gamma} M_0}{u} \tag{25d}$$

In summary three parameters will be varied in the present research. They are ϕ_T, ϕ_K and R^*, while the isentropic index and the overdrive are fixed at 1.2, and the non dimensional heat release is taken equal to the non-dimensional activation energy. Note that the reference value $Q_{ref} = 25$ yields an adiabatic flame temperature of $T_{ad} = 1550K$ in standard conditions. Different cases will be denoted by defining the values of R^*, ϕ_K (or the Damkhöler number itself) and E, as this yields a more compact notation.

V.E. Discretization

Equations (17) and (20) are discretized in the x direction using the Chebyshev tau method, Dongarra, *et al.*[7] Denoting by N the order of the maximum Chebyshev polynomial resolved in the truncation error, and $C_k(x)$ the Chebyshev polynomial of the k_{th} order, the expansion takes the form:

$$z_j = \sum_{k=0}^{N+1} \hat{z}_{j,k} C_k(\xi), \tag{26}$$

where $\hat{z}_{j,k}$ is the array of Chebyshev components. The time integration is carried out using a variable step stiff ODE solver, with maximum absolute tolerance set to 1×10^{-7}. A second order A-stable time integrator has been used to advance the solution in time. It was determined that A-stability is a necessary property to accurately resolve the dynamics of time-unstable detonations.

The solution domain is decomposed in two regions, marked as (1) and (2) in Fig. 1(b). In each region 175 Chebyshev polynomials are used to represent the solution. Numerical convergence of the Chebyshev expansion is monitored in three ways: i) for longitudinally stable detonations, the detonation Mach number of the zeroth order solution approaches at large times the ZND value, the maximum relative error in detonation Mach number for $E = Q < 18.39$ is 1.35×10^{-4}; ii) the growth rate of the surface deformation a_1 matches for large time the values given by the linear analysis on 1D detonations. This point will be discussed in more detail in the following; iii) a grid convergence study was conducted on the numerical solution. The solutions converging at the slowest rate were determined to be those at highest activation energy and highest Damkhöler number, low ϕ_K. The absolute convergence error for $E = Q = 25$ and $\phi_K = 0.1$ is shown in Fig. 6. Note that large error for large times are due to the instability growth. The error suddenly increases around $t = 1.2$ because of the formation of a shock in the reactive mixture. Finally, the maximum relative error between the $N = 200$ and the $N = 175$ is equal to 0.027.

VI. Results

For each value of the scaled activation energy, *i.e.*, ϕ_T, two isentropic solutions, denoted as frozen and equilibrium cases will be considered together with the finite Damkhöler number ones. The frozen solution corresponds to setting $\lambda = 0$ in equation (10), while the equilibrium solution corresponds to $\lambda = 1$. It would be desirable to identify the two isentropic cases with limits in the Damkhöler number. Our analysis shows that the frozen solution corresponds to the limit $Da \to 0$ for the reactive RMI problem, while the equilibrium solution does not correspond to the $Da \to \infty$ limit. The rationale is that as Da increases at constant activation energy and heat release, the term $\lim_{t \to 0^+} \left(\frac{\partial P^0}{\partial \tau} + R\left(P^0\right) \right)$ increases in a proportional manner, leading for $Da \to \infty$ to an infinitely large initial perturbation. For $Da \gg 1$ and $\delta^0 \ll 1$ the second term in equation (20) becomes the dominant contribution to the perturbation growth. Physically such term corresponds to the contribution to the perturbation dynamics of the spatial derivative of the solution at $t = 0$, and the y variation of the impact time between the incident shock and the contact discontinuity. In fact, according to equation (19), δ^1 is proportional to the difference in surface deformation between the transmitted shock and the contact discontinuity, while, according to equation (23), the initial difference in deformation is proportional the ratio in velocity between incident and transmitted shock.

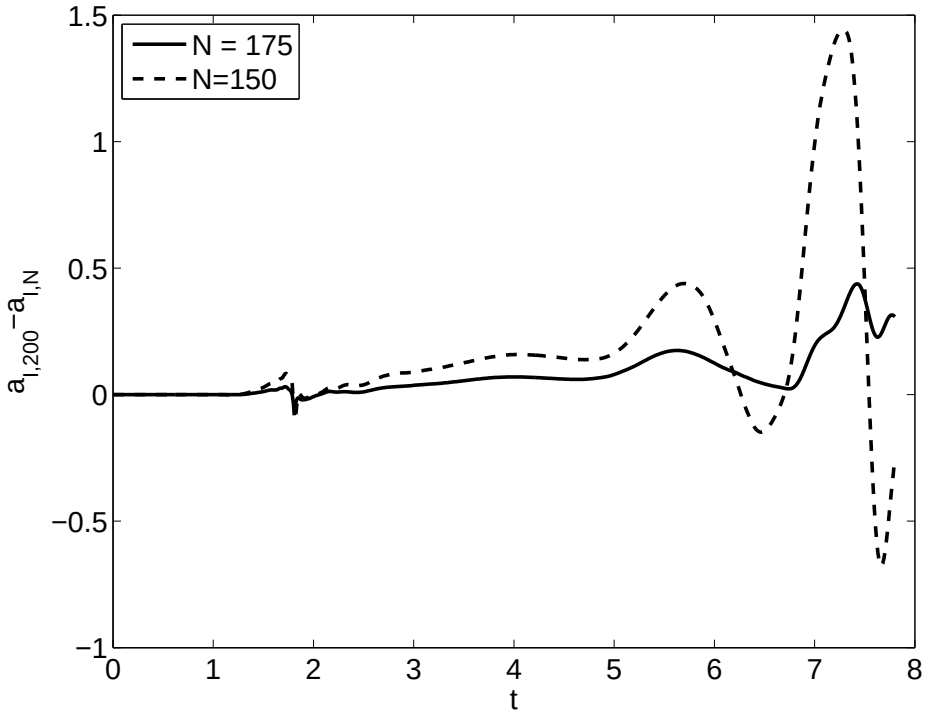

Figure 6. Convergence error for $E = Q = 25$ and $\phi_K = 0.1$ and two values of the Chebyshev expansion order N.

The magnitude of the initial perturbation scales linearly with the Damkhöler number, being the reaction length the only length scale of the 0th order perturbation. It also increases with heat release and decreases with the non-dimensional activation energy. In Fig. 7 we show the effect of the activation energy on the surface deformation rate, $\lim_{t\to 0^+} \dot{a}_2$, for two Q values, $Da = 1$, and with the remaining parameters set as described in §V.D.

The influence of E and ϕ_K on the deformation growth rate of the contact discontinuity is shown in Fig. 8. The end time of the simulations is set to 15. Cases for which a free detonation is unstable were stopped for $t < 15$ when the deformation of the transmitted shock, a_1 reached the value of 1000. Considering the two isentropic solutions, the reactivity acts to increase the deformation rate because, given identical incident conditions, the transmitted shock travels faster than the non-reactive analog, *i.e.*, the shock induced acceleration is stronger. The initial v^1 jump across the interface is larger in the reactive case. For the finite Damkhöler number cases the acceleration of the shock takes place over a finite time interval. For medium Damkhöler numbers the reactive solutions support a larger deformation rate than the non reactive analogs. This is especially evident in the linear growth phase, *i.e.*, at large times $t \to \infty$. A decrease in activation energy accentuates the decrease in linear growth rate at large Damkhöler numbers. For small times, large Damkhöler solutions support a large growth rate. This phenomenon is linked to the increase in initial rate previously described in conjunction with Fig. 7. The small time variation of $\dot{a}_2$ versus t is shown in Fig. 9 for four values of ϕ_k and $E = Q = 10$.

The detonation instability manifest itself by altering the linear regime at large t. Below the longitudinal instability limit, $E < 18.39$, for low value of ϕ_k a free detonation is stable. The instability boundary ϕ_k versus E is shown in Fig. 10.

The effect of detonation instability on the contact-surface deformation a_2 is enhanced at high activation energies and low wave numbers, ϕ_k (*i.e.*, high Damkhöler numbers). The reason for the deformation/activation energy correlation is the higher instability growth rate at higher energies. Note that in our analysis when changing the activation energy the time scale changes, because the mixture is maintained fixed.

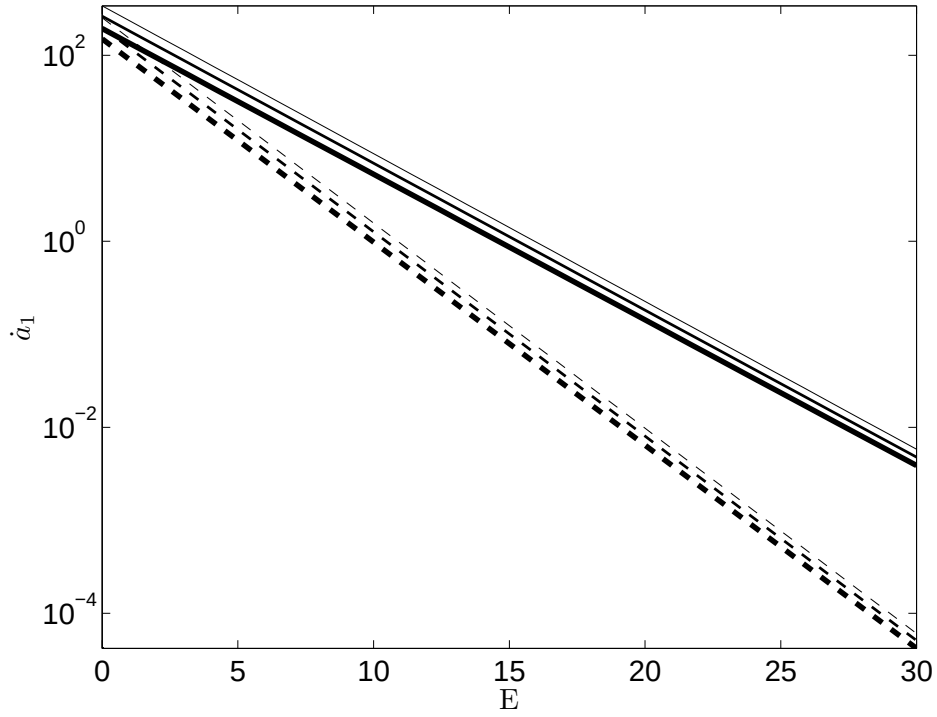

Figure 7. Initial deformation rate versus E for two values of Q and three values of R^*, $f = 1.2$, $\gamma = 1.2$, $Da = 1$. Note, logarithmic y scale. Solid lines $Q = 30$, dashed lines $Q = 15$. Thin lines $R^* = 2/3$, medium lines $R^* = 1/2$ and thick lines $R^* = 1/3$.

So the above mentioned relationship must be intended as equivalent to saying that the growth rate increases with respect to the time scale that controls the non-reactive RMI. The reason for the deformation/wave number trend is the finite time necessary for the instability development.

The transmitted shock deformation a_1 is significantly more pronounced at large time than the contact discontinuity. The exponential increase proper of unstable free detonations is recovered at large times. The deformation rate of the transmitted shock is compared to the free detonation highest normal mode eigenvalue (complex), $\bar{\alpha}$, by minimizing the L_2 norm,

$$\left\| a_1 - C_3 \exp\left(C_1 \tau\right) \sin\left(C_2 \tau + C_4\right) \right\|, \quad \tau \in [t, t - 2\pi/\Im\left(\bar{\alpha}\right)],$$

in the vector C_i. The estimated growth rate is $\alpha(t) = C_1$. The ratio $\alpha(t)/\Re\left(\bar{\alpha}\right)$ is plotted versus time in Figs. 11 and 12 for four values of the activation energy and ϕ_k. For the eight cases shown in Figs. 11 and 12 $\bar{\alpha}$ is given in table (1). We thus summarize the results of the growth rate analysis by noticing that stronger contact interface deformation correlate with stronger transmitted shock deformation and are caused by an increased free detonation instability. For detonations with a low $\bar{\alpha}$ the transmitted shock interface still exhibits an exponential growth rate, but the contact interface manifest the linear growth at large time proper of the RMI.

To characterize the effect of velocity on the large time contact interface growth rate we focus on the smallest wave number analyzed, $\phi_k = 0.1$, and determine the least squares fit to $a_2(t)$ for $t > 5$ for different activation energies. The slope of this fit is scaled by the asymptotic value $\lim_{t\to\infty} \dot{a}_2$ for the inviscid RMI, and shown in Fig. 13. The results imply that the late stage slope increases with the activation energy. The rationale is a decreasing value of the perturbation velocity u^1 in the reactive region following the explosion. For small values of the activation energy the terminal slope is lower than the non-reactive analog.

Finally the effect of a change in the density ration R^* for small wave numbers is illustrated in Fig. 14. An increase in density ratio increases the early stage contact-surface deformation and decreases the late stage deformation rate. The results in Fig. 14 are in agreement with those in Fig. 7, where the initial

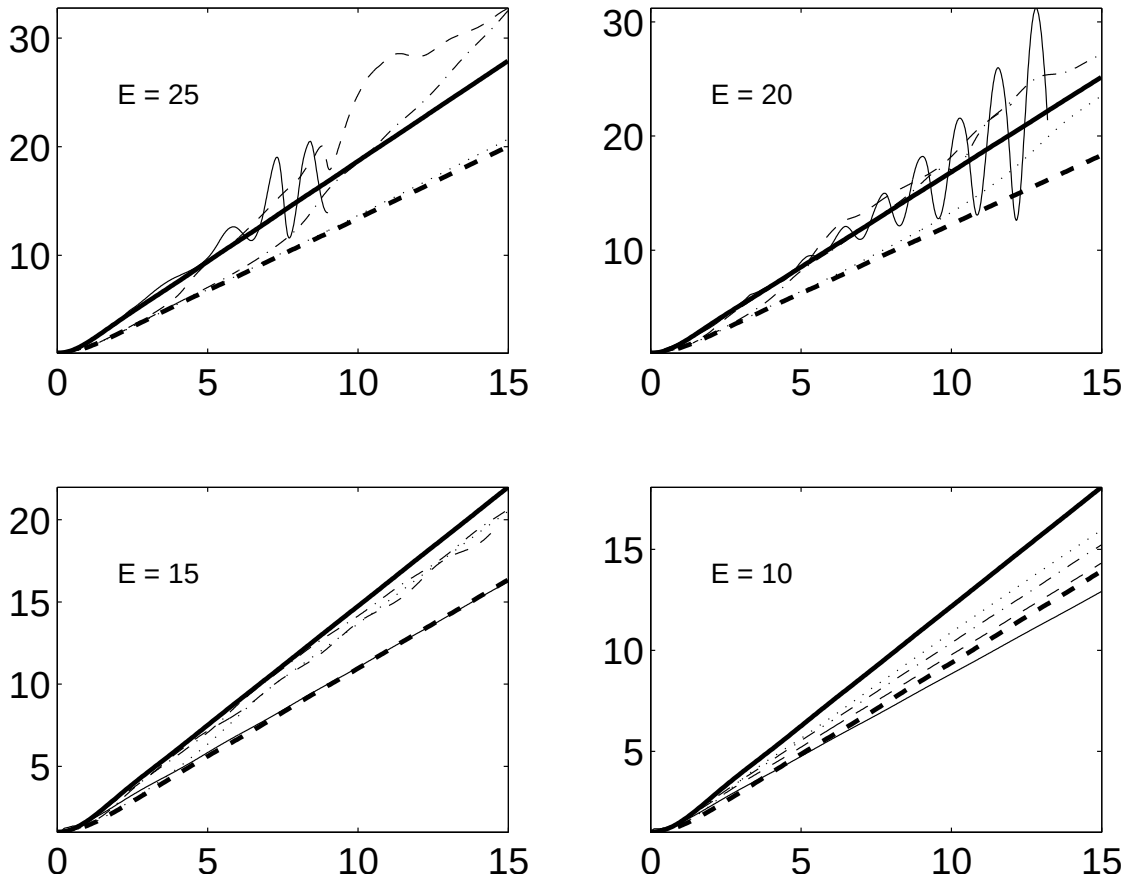

Figure 8. Interface deformation versus time for four values of E. The two thick lines represent the isentropic cases: the dashed line is the non-reactive solution. The thin lines are: — $\phi_k = 0.1$, - - $\phi_k = 0.5$, -· $\phi_k = 1$ and $\cdots$ $\phi_k = 3$.

E	$\bar{\alpha}$	$\bar{\alpha}$
25	1.6557 @ $\phi_k = 0.25$	1.1145 @ $\phi_k = 0.5$
20	1.2415 @ $\phi_k = 0.25$	1.0425 @ $\phi_k = 0.5$
15	0.57493 @ $\phi_k = 0.5$	0.61259 @ $\phi_k = 1$
10	0.045019 @ $\phi_k = 1$	0.233 @ $\phi_k = 1.5$

Table 1. Growth rates for free propagating detonations.

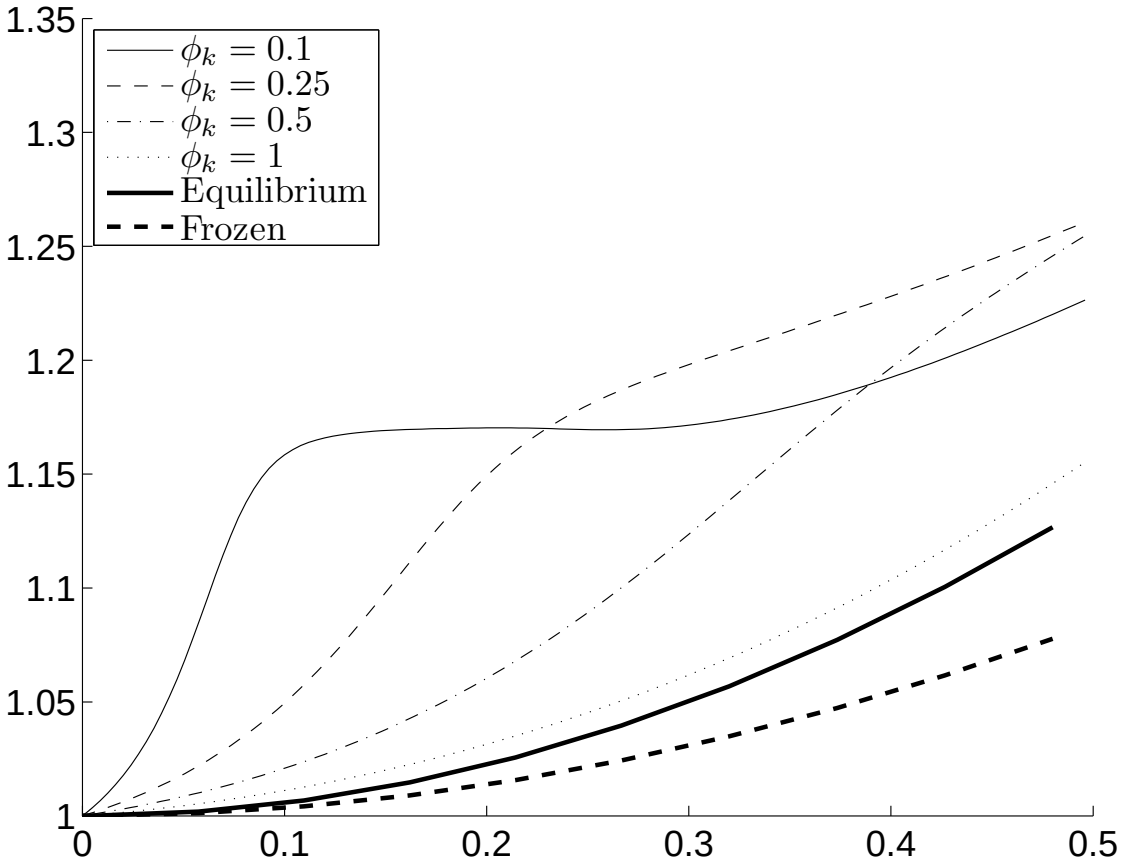

Figure 9. Interface deformation versus time for four values of ϕ_k and $E = 10$.

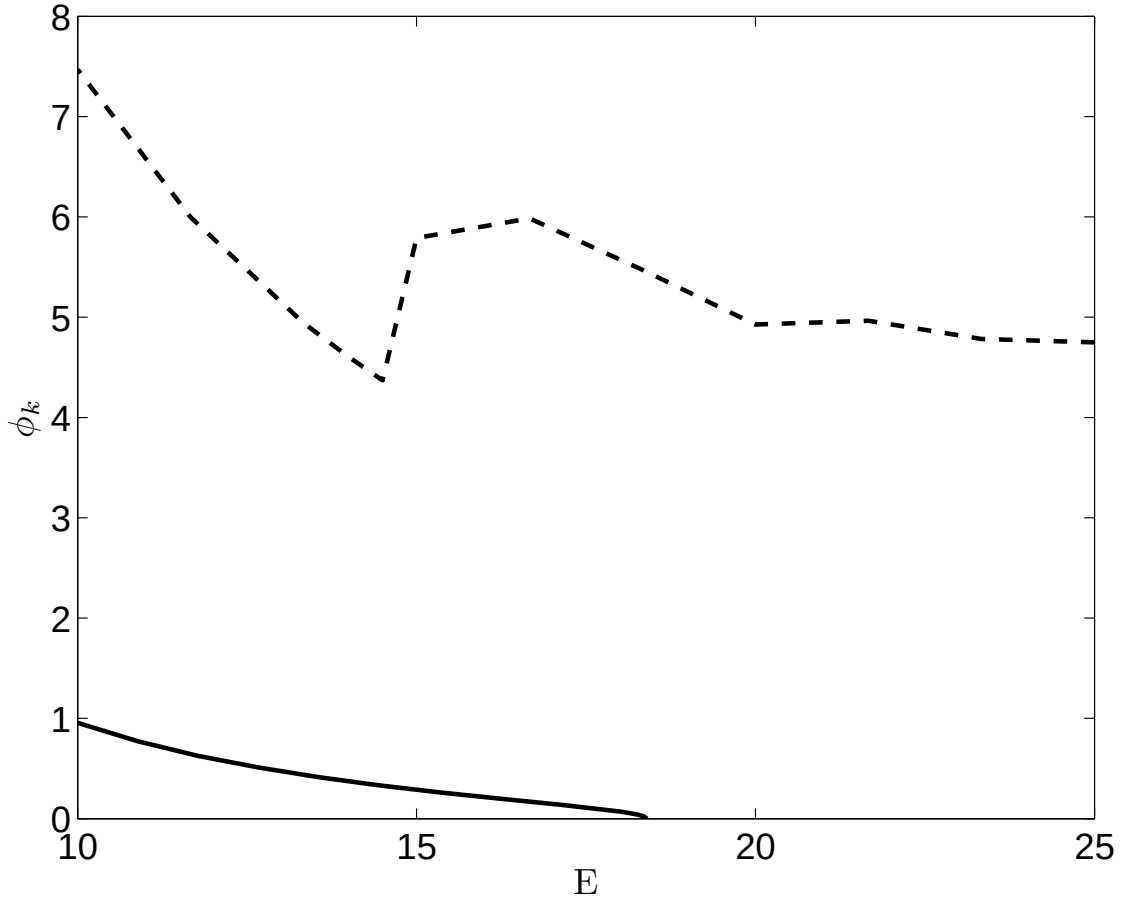

Figure 10. Stability boundary for a free detonation with $\gamma = f = 1.2$.

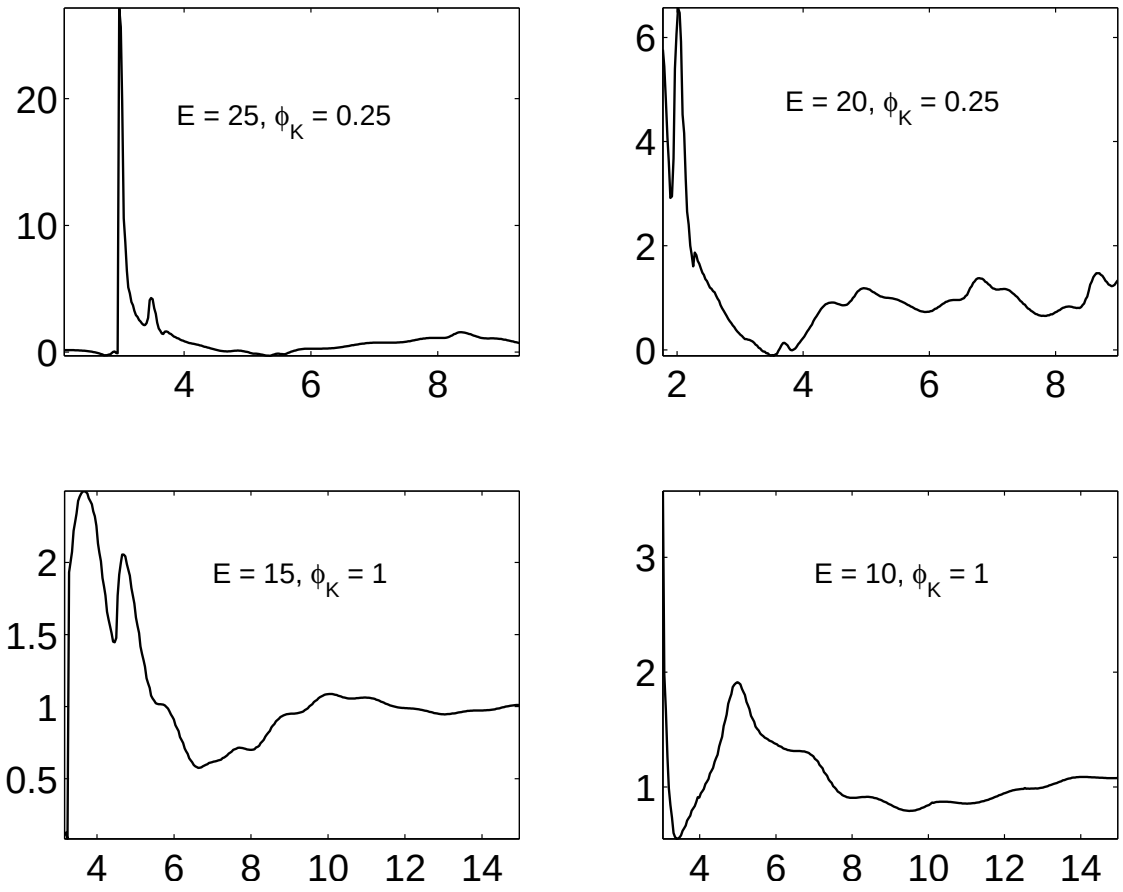

Figure 11. Scaled growth rate versus time, a different set of wave numbers.

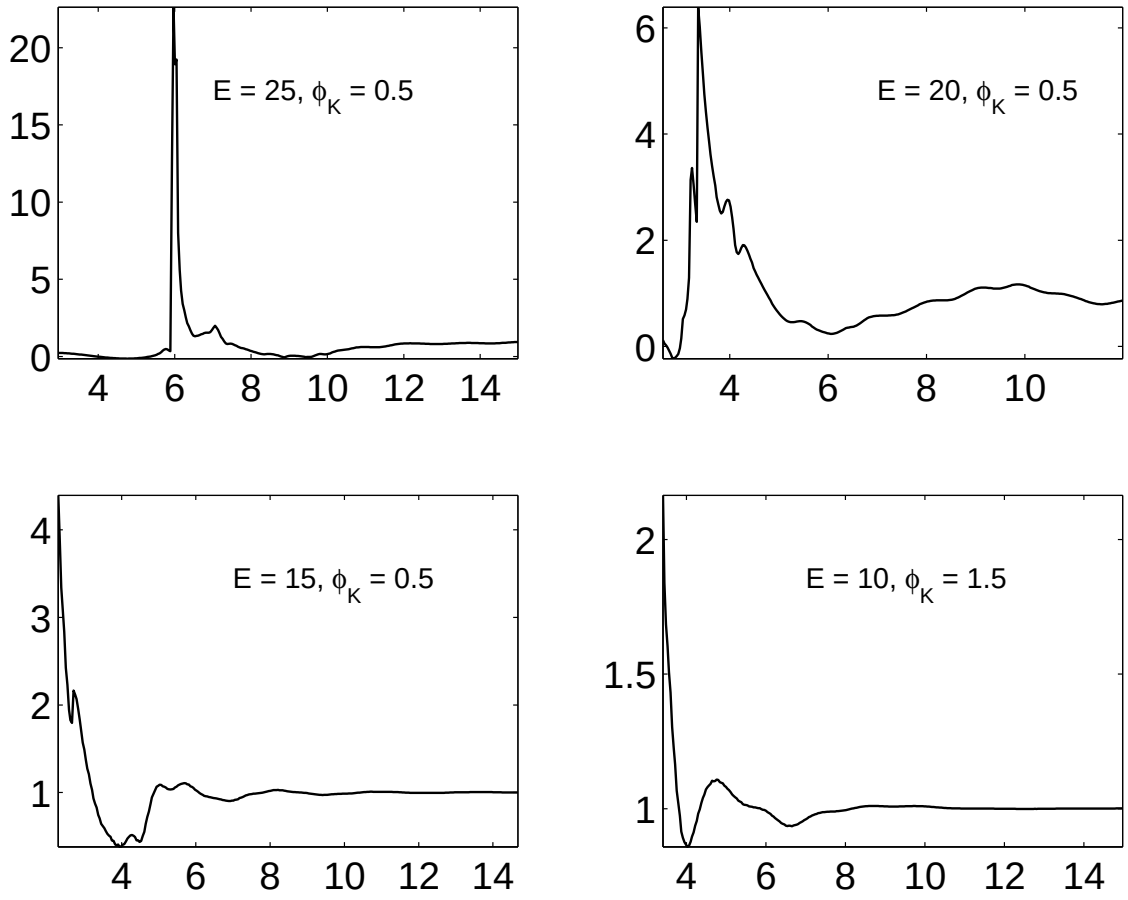

Figure 12. Scaled growth rate versus time.

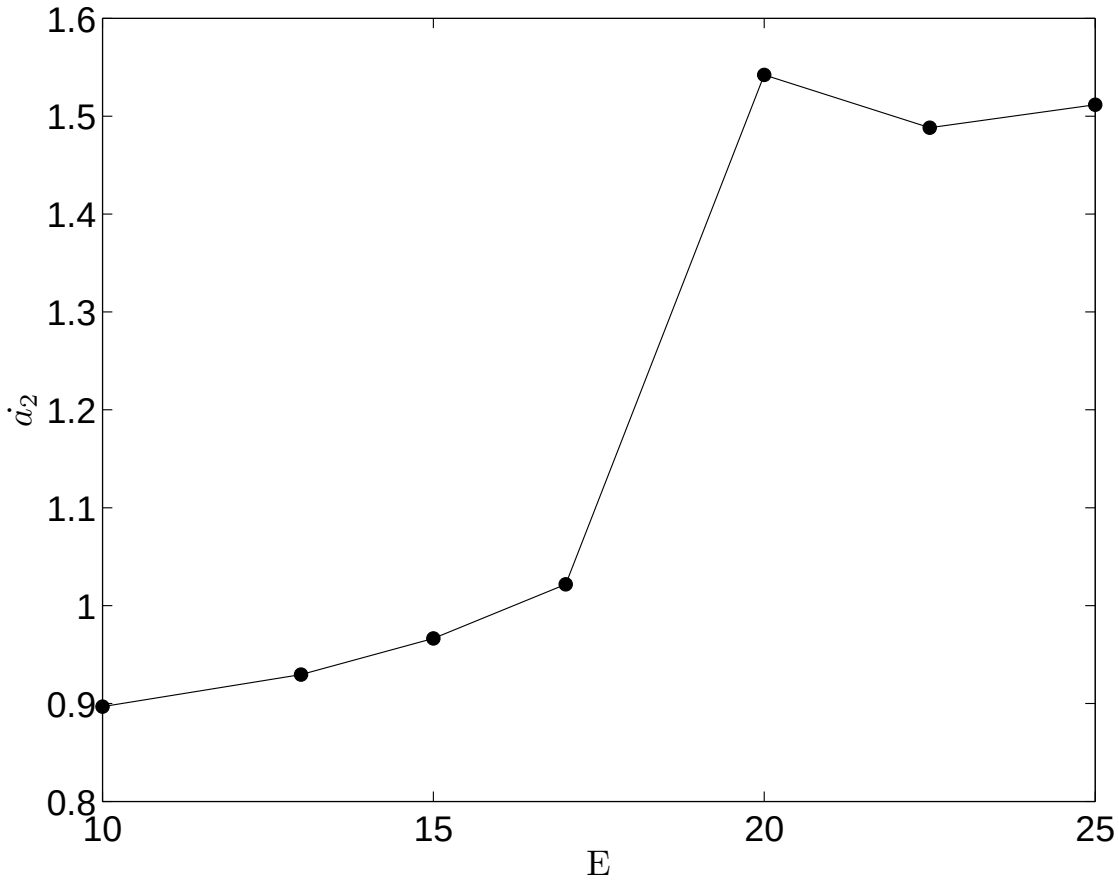

Figure 13. Late stage slope (*i.e.*, best fit of $a_2(t)$ for $t > 5$) versus activation energy.

deformation rate was shown to increase with R^*. The negative correlation between linear (late stage) and initial growth rate confirms our previous results, thus allowing us to extend our conclusions to density ratios in a neighborhood of $R^* = 1/2$.

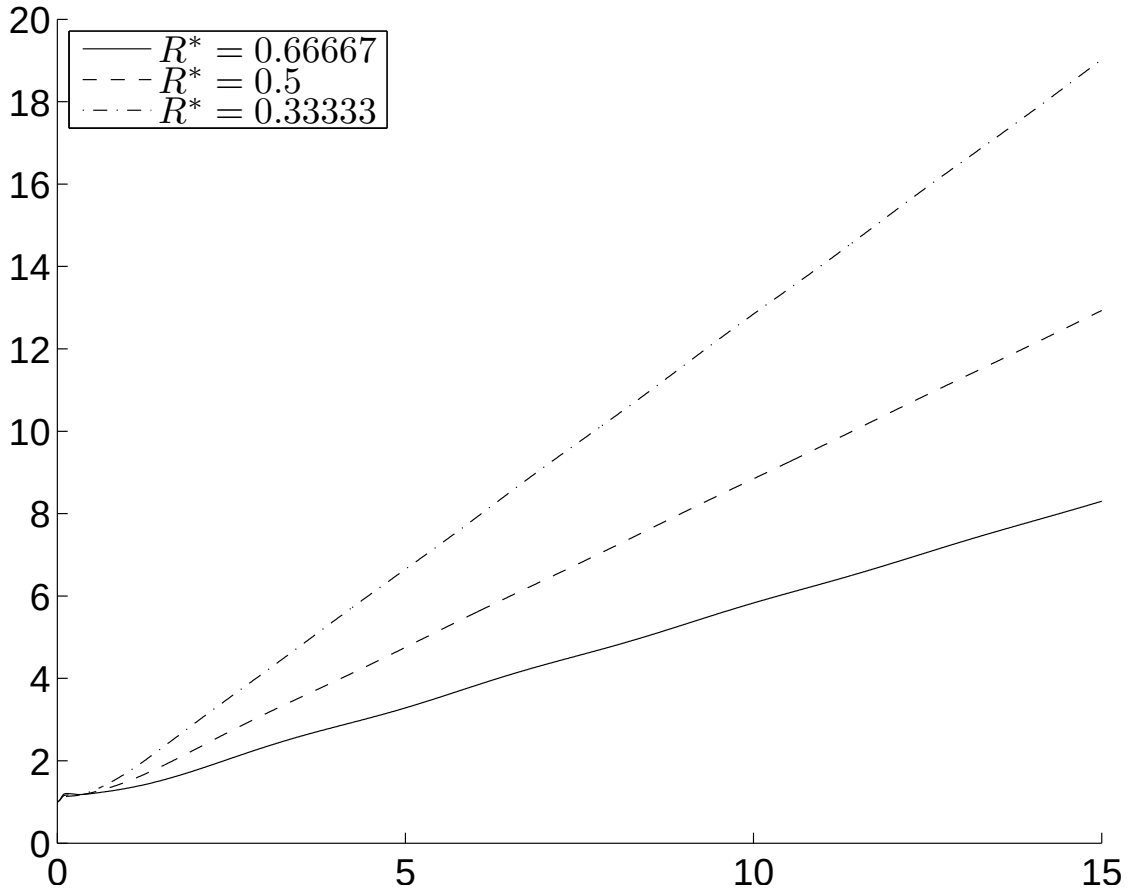

Figure 14. Interface deformation versus time for $\phi_k = 0.1$, $E = 10$ and three values of R^*.

VII. Conclusion

In this paper we analyze the instability generated by an incident shock traveling from a light non-reactive fluid into a heavy reactive one. The Richtmyer-Meshkov instability (RMI) for reactive mixture presents two specific features that explain the parametric influence of the reactivity, *i.e.*, Damkhöler number. The first is associated with the initial acceleration of the interfaces over a spatially varying field, and induces a strong variation of the contact interface deformation with the wave number for short times. The long time linear growth rate correlates negatively with the initial growth rate.

The second is associated with the correlation between free detonation instability and RMI. Exponential growth of the interface is observed only for highly unstable detonations, while the linear growth due to the RMI dominates for low activation energy and heat release. The transmitted shock manifest an exponential growth very similar to that of free detonations.

References

[1]Richtmyer. Taylor instability in shock acceleration of compressible fluids. *Comm. Pure Appl. Math.* XIII:297, (1960).

[2]Khokhlov, Oran, Chtchelkanova and Wheeler. Interaction of a shock with a sinusoidally perturbed flame. *Combust. Flame* 117:99, (1999).

[3]Khokhlov, Oran and Thomas. Numerical simulation of deflagration to detonation transition: The role of Shock-Flame interaction in turbulent flames. *Combust. Flame* 117:323, (1999).

[4]Massa and Lu. Role of the induction zone on turbulence-detonation interaction. *Physics of Fluids* under review:, (2008).

[5]Tomkins, Kumar, Orlicz and Prestridge. An experimental investigation of mixing mechanism in shock accelerated flow. *J. Fluid Mech.* 611:131, (2008).

[6]Erpenbeck. Stability of Idealized one-reaction Detonations. *Physics of Fluids* 7(5):684, (1964).

[7]Dongarra, Straughan and Walker. Chebyshev tau-QZ algorithm methods for calculating spectra of hydrodynamic stability problems. *Appl. Num. Math.* 22:399, (1996).